HYDROTHERMAL CHARACTERISTICS OF A COLD REGIONAL TUNNEL UNDER DIFFERENT CLIMATIC SCENARIOS

by

Haiqiang JIANG[a,b,c], Tengfei ZHOU[a,b], Enliang WANG[a,b], Fujun NIU[c,d*], Jiarui HE[a], Junlin HE[c], Yongdong LI[c], and Wangtao JIANG[c]

[a] School of Water Conservancy and Civil Engineering, Northeast Agricultural University, Harbin, China
[b] Heilongjiang Provincial Key Laboratory of Water Resources and Water Conservancy Engineering in Cold Region, Northeast Agricultural University, Harbin, China
[c] South China Institution of Geotechnical Engineering, South China University of Technology, Guangzhou, China
[d] State Key Laboratory of Subtropical Building Science, South China University of Technology, Guangzhou, China

Original scientific paper
https://doi.org/10.2298/TSCI230122122J

Cold regional tunnels have been encountering numerous frost damages as a result of dynamic changes in hydrothermal conditions of tunnel structural layers. The climate change is recognized as a major contributor for the problems. In this study, the hydrothermal conditions of a high speed railway tunnel are evaluated under different climate scenarios based on in-situ data and numerical analysis. Subsequently, the effect of different thicknesses of insulation board on hydrothermal conditions inside the tunnel is compared and the reasonable thickness is obtained. The main findings are: The temperature and unfrozen water content gradually decreased and the ice content gradually increased with the service time of the tunnel in the early 15 years; the maximum frozen depth occurs at the tunnel sidewall and it with a depth of 1.64 m within 30 years after the construction. The hydrothermal conditions inside the tunnel are significantly affected by annual mean air temperature (AMAT) and annual range of air temperature (ARAT); the maximum frozen depth decreases with AMAT, but increases with ARAT. After the XPS board with a thickness of 5 cm is laid in tunnel structural layers, the temperature at the most unfavorable position is 0.55 °C in the cold season, which suggests that frost damages disappeared and this method can be used to protect the tunnel against the frost damages. This paper can provide a basis for heat insulation design of the cold regional tunnels.

Key words: *cold regions, tunnel, climatic changing, frost damages, numerical analysis*

Introduction

Cold regions are defined as the areas where the mean air temperature during the coldest month of a complete year remains below 0 °C [1]. Cold regions are widely distributed in the world, which account for approximately 50% of total terrestrial area [2]. Particularly, this value can reach 43.5% in China [3]. In cold regions, the problem soils including seasonally frozen ground and permafrost ground frequently encounter with larger amounts of practical en-

* Corresponding author, e-mail: niufj@scut.edu.cn

gineering. On the other hand, with the increase in the extent of human activities, a large number of traffic engineering have been built in the regions, such as the Lanzhou-Xinjiang high speed railway, the Qinghai-Tibet railway and the Harbin-Dalian high speed railway, *etc*. Due to the influence of extreme climate, these projects are subject to serious damages to varying degrees during operating period, such as frost heave deformation, thawing and subsidence of roadbed and uneven settlement of bridge transition section, *etc*. [4-11]. As a main part of traffic engineering, tunnels are also inevitably threated by a series of problems wherein the icing of vaults, cracking of side walls, freezing of drainage ditches and snow accumulation at tunnel portal [12-16]. Those damages can significantly reduce the service life of the tunnels, interrupt traffic or even cause the tunnel to be scrapped. By 2021, the total length of tunnels has exceeded 19630 km in China [17]. In the future, this number will continue to increase. Thus, the significance of preventing the frost damages in tunnels is more prominent. How to avoid and migrate frost damages inside the tunnel is closely linked to hydrothermal conditions of surrounding rocks and tunnel structures. Therefore, understanding the change process of hydrothermal conditions is a basis for preventing frost damages and improving the service life of cold regional tunnels.

In-situ monitoring and numerical simulation are the most common methods to study the hydrothermal conditions of cold regional tunnels. Jiang *et al*. [18] concluded that the thermal characteristics inside the tunnel are associated with topography, environment and the synergy of tunnel directions. Chang *et al*. [19] recorded the temperatures of air, surrounding rocks and tunnel structures in long-term, which showed the thermal characteristics of the tunnel were affected by traffic-induced thermal effect. Liu *et al*. [20] monitored the temperature distributions of four cross-sections in a permafrost tunnel, indicating that the amplitude of air temperature in the tunnel decreases gradually as the distance from the entrance to the exit increases. Zhao *et al*. [21] proposed a novel distributed temperature monitoring system to test the temperature distributions at fire-proof, thermal insulation board surface, sidelining and lining surface of a cold regional tunnel, which reveals that the temperature at thermal insulation surface and inside tunnel change slightly compared with the other locations. Besides, the tunnel temperature variation distributes along the longitudinal direction and also changes with the seasons [16]. The conclusions drawn in previously mentioned literatures by in-situ monitoring provide the comprehensive and immediate thermal conditions and plays a guiding role in the tunnel design for the cold regional tunnels.

However, the cost of in-situ monitoring is expensive and time-consuming. With the development of computer technology and theories related to heat and mass transfer, numerical simulation becomes popular. In this regard, most scholars have focused on numerical models considering the influence of ventilation, piston action as well as multi-physics coupling. Yan *et al*. [22] provided a reference on frost prevention in cold regional tunnels by analyzing the design parameters of insulation layer under different mechanical ventilation conditions. Jiang *et al*. [23, 24] studied the effect of piston action caused by train running on thermal environment inside the tunnel, and found that air temperature distribution depended on air temperature outside the tunnel and train speed. Meanwhile, as the piston action accelerates heat exchange between the air inside and outside the tunnel, the frozen depth at tunnel portal is much bigger than that at tunnel middle section. Yang *et al*. [25] established a hydro-thermal coupling model for cold regional tunnel considering heat transfer and water ice phase. Jiang *et al*. [26] investigated the influence of performance degradation of insulation board on hydrothermal conditions and evaluated the difference between two insulation measures. The valuable researches about the cold regional tunnels based on numerical analysis include but are not limited to aforementioned, which gives guidelines for preventing frost damages of tunnels. Some anti-freezing measures were proposed, such as laying insulation board

in tunnel structural layers, installing electric heat tracing at secondary lining surface and installing air curtains at tunnel portal, and the excellent effects of those measures have been confirmed by many cases. Yuan [27] analyzed the temperatures of secondary lining and primary support of a tunnel, and revealed that the temperatures inside the tunnel significantly increased after using the foam concrete with high strength and thermal insulation. Lai *et al*. [28] combined the electric tracing technology and insulation layer to prevent the tunnel structural layers from frost damages. Wang *et al*. [29] found that temperature inside the tunnel significantly increased after installing the air curtain while frost damage disappeared in cold season. However, most of aforementioned researches are focused on ordinary railway tunnel instead of high speed railway tunnel. The deformation of high speed railway tunnels is stricter than the ordinary railway tunnels (the settlement of high speed railway must be less than 15 mm after construction) [30]. On the other hand, the global climatic warming becoming an unavoidable issue for the railways in cold regions. In the Qinghai-Tibet plateau [31, 32] and northeast of China [33, 34], the permafrost degrading caused by climatic warming reduces the bear capacity of the subgrade soils and further causes disasters [35]. At present, the occurrence of the disasters is still with high frequency and serious severity [36, 37]. Similarly, the influence of climatic changes on cold regional tunnel also cannot be ignored.

To fill the gaps, the hydrothermal conditions of a high speed railway tunnel located in northeast of China considering climatic change are investigated based on in-situ monitored data and numerical analysis. The aims of this study are to:

– determine the evolution of hydrothermal conditions inside the tunnel under different climatic scenarios,
– quantify the relationship between maximum frozen depth and AMAT as well as ARAT, and
– obtain the reasonable thickness of insulation layer for the cold regional tunnels.

This paper can help us understand the change process of hydrothermal conditions and provide some guidelines for the design and construction of high speed railway tunnels in cold regions.

In-situ monitoring

Study site

The Jilin-Tumen-Hunchun passenger dedicated line (JTHPDL) was constructed in 2015 and it is located in the northeast of China. The studied tunnel is Gaotai tunnel located in Antu County, Jilin province. The total length of the tunnel is 3706 m and the slope is 12.4‰, as shown in fig. 1. Fully weathered granite, strongly weathered granite and weakly weathered granite are stratified from the summit to the base of the mountain. The groundwater is mainly

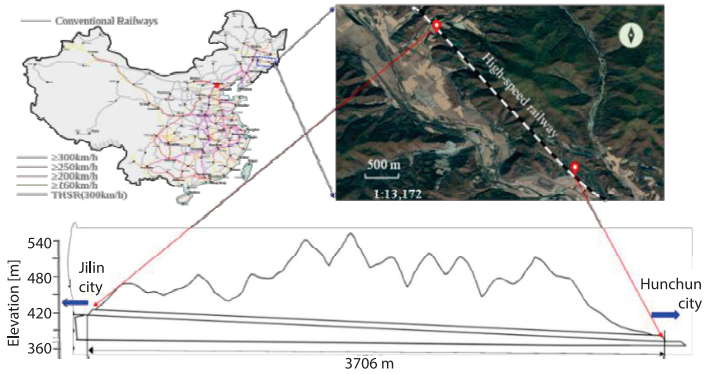

Figure 1. Basic information of studied tunnel [38]

quaternary rock pore water and bedrock fissure water. The groundwater depth is generally between 0.0 m and 5.0 m and the seasonal variation ranges from 0.5-2.0 m. The maximum buried depth is 188.0 m.

In-situ monitoring design

The in-situ monitoring system consists of the monitoring system inside the tunnel and outside the tunnel. The monitoring system inside the tunnel is composed of the temperature sensors, the meteorological sensor with five parameters, and the data logger, as shown in fig. 2. These instruments were mainly used to record air temperature inside the tunnel, the temperatures of tunnel structural layers and the surrounding rocks. The monitoring system inside the tunnel was powered by electricity. The monitoring system outside the tunnel was installed near the entrance and exit of tunnel, which was mainly used to record ground temperature and air temperature at the tunnel portal. All temperature sensors were calibrated based on the related standard [39]. The record frequency of the data logger is twice per hour.

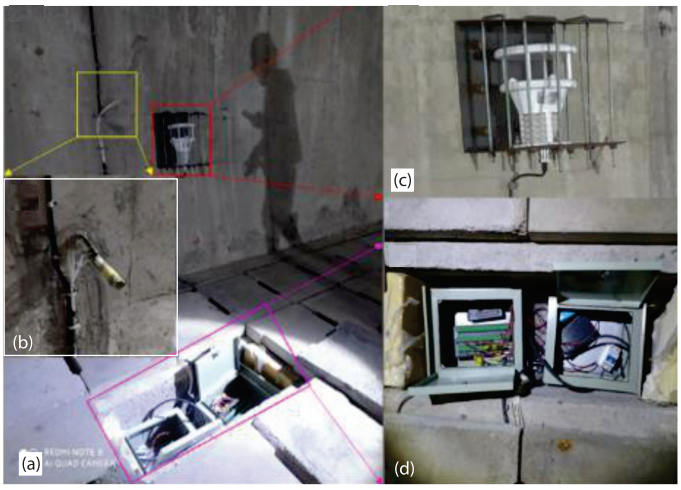

Figure 2. The monitoring system inside the tunnel; (a) the monitoring system inside the tunnel, (b) temperature sensor, (c) the meteorological sensor with five parameters, and (d) data logger [40]

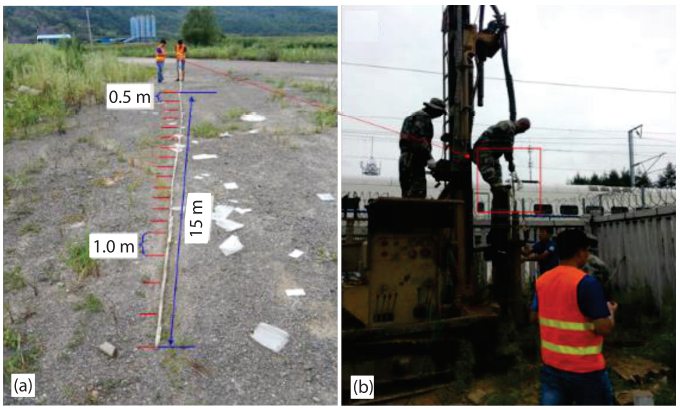

Figure 3. Installation of monitoring points at tunnel portal

The temperature gradient near ground surface is larger due to the presence of the boundary-layer. Therefore, the distance between adjacent temperature sensors in the depths ranging from 0-10 m is fixed at 0.5 m. When the depth exceeds 10 m, the spacing between adjacent temperature sensors is 1 m. All temperature sensors were tied on a wood strip, as is shown

in fig. 3(a). Afterward, a bore with the depth of 15 m was excavated by a drilling rig and then put the wood strip inside the bore, fig. 3(b). Finally, the bore was backfilled with sand.

The tunnel profile and locations of temperature sensors along the tunnel radial direction are shown in fig. 4. The temperature sensors were arranged at three different positions, one sensor was installed 5 cm away from secondary lining surface to monitor air temperature, and the two reminding sensors were installed at the center of secondary lining and the interface between secondary lining and primary support to monitor temperatures at corresponding points, respectively.

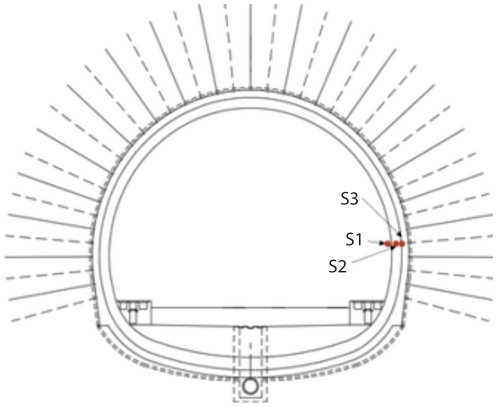

Figure 4. Tunnel profile and locations of monitoring points: *S1 – the air temperature, S2 – the temperature at the center of secondary lining, and S3 – the temperature at the interface between secondary lining and primary support*

Numerical model

Governing equation

The coupled hydrothermal model was developed considering heat transfer and ice phase. The governing equations should satisfy the following assumptions:

- The surrounding rocks are homogeneous and isotropic.
- Ice is incompressible.
- The convective heat generated by water migration is ignored.
- Water migration obeys the Darcy's law in both frozen and unfrozen zones.

The heat transfer equations in the thawed and frozen zones can be expressed [41]:

$$c_u \rho_2 \frac{\partial T_u}{\partial t} = \frac{\partial}{\partial x}\left(\lambda_u \frac{\partial T_u}{\partial x}\right) + \frac{\partial}{\partial y}\left(\lambda_u \frac{\partial T_u}{\partial y}\right) \tag{1}$$

$$c_f \rho_2 \frac{\partial T_f}{\partial t} = \frac{\partial}{\partial x}\left(\lambda_f \frac{\partial T_f}{\partial x}\right) + \frac{\partial}{\partial y}\left(\lambda_f \frac{\partial T_f}{\partial y}\right) + L\rho_i \frac{\partial \theta_i}{\partial t} \tag{2}$$

where f and u are the medium in frozen and thawed states, respectively, λ – the thermal conductivity, T – the temperature, t – the time, c – the specific heat capacity, ρ_2 and ρ_i are density of medium and ice, respectively, L – the latent heat of phase transition, and θ_i – the volumetric ice content.

The water migration caused by air and water vapor can be ignored as it is limited in quantity. At this point, the mass transport of unsteady flow during the freeze-thaw process in surrounding rocks can be expressed:

$$\frac{\partial \theta_u}{\partial t} + \frac{\rho_i}{\rho_w}\frac{\partial \theta_i}{\partial t} = \frac{\partial}{\partial x}\left(K\frac{\partial \varphi}{\partial x}\right) + \frac{\partial}{\partial y}\left(K\frac{\partial \varphi}{\partial y} + K\right) \tag{3}$$

where K is hydraulic conductivity, φ – the matrix potential, and θ_u – the volumetric content of unfrozen water.

The relationship between temperature and unfrozen water content can be determined:

$$\theta_u = a_1 \left|T_f\right|^{-b_1} \tag{4}$$

$$b_1 = \frac{\ln\theta_0 - \ln\theta_u}{\ln|T| - \ln|T_m|} \tag{5}$$

$$a_1 = \theta_0 T_m^b \tag{6}$$

where θ_0 is the initial water content of the surrounding rocks, that is 15% for the study tunnel and a_1 and b_1 are empirical constants of $6.989 \cdot 10^{-2}$ and –0.26, respectively.

The moisture diffusion coefficient is shown:

$$D = \frac{K}{C} \tag{7}$$

The water migration equation can be expressed:

$$\frac{\partial\theta_u}{\partial t} + \frac{\rho_i}{\rho_w}\frac{\partial\theta_i}{\partial t} = \frac{\partial}{\partial x}\left(D\frac{\partial\theta_u}{\partial x}\right) + \frac{\partial}{\partial y}\left(D\frac{\partial\theta_u}{\partial y} + K\right) \tag{8}$$

Then the θ_i can be removed and the heat transfer equation can be further expressed:

$$\begin{aligned}\left(c_f\rho_2 + L\rho_w\frac{\partial\theta_u}{\partial T_f}\right)\frac{\partial T_f}{\partial t} &= \frac{\partial}{\partial x}\left(\lambda_f + L\rho_w D\frac{\partial\theta_u}{\partial T_f}\right)\cdot \\ \cdot\frac{\partial T_f}{\partial x} + \frac{\partial}{\partial y}&\left(\lambda_f + L\rho_w D\frac{\partial\theta_u}{\partial T_f}\right)\frac{\partial T_f}{\partial y} + L\rho_w\frac{\partial K}{\partial y}\end{aligned} \tag{9}$$

The heat conduction equation of surrounding rocks considering ice-water phase and water migration is further determined by equivalent substitution method and can be expressed:

$$C^e\frac{\partial T}{\partial t} = \frac{\partial}{\partial x}\left[\lambda_x^e\frac{\partial T}{\partial x}\right] + \frac{\partial}{\partial y}\left[\lambda_y^e\frac{\partial T}{\partial y}\right] \tag{10}$$

where λ^e and C^e are the equivalent thermal conductivity and equivalent specific heat capacity, respectively. When the surrounding rocks is thawed ($T \geq T_m$), $C^e = c\rho_2$, $\lambda^e = \lambda_u$. When the surrounding rocks is frozen ($T < T_m$),

$$C^e = c_f\rho_2 + L\rho_w\frac{\partial\theta_u}{\partial T},\ \lambda^e = \lambda_f + L\rho_w D\frac{\partial\theta_u}{\partial T}.$$

In this study, the required parameters of tunnel structural layers are listed in tab. 1.

Table 1. The required parameters of tunnel structural layers [26]

Parameters	Density [gcm^{-3}]	Thermal conductivity [Wm^{-1}°C^{-1}]		Heat capacity [kg°C]	
		Frozen state	Thawed state	Frozen state	Thawed state
Surrounding rocks	2590	2.27	1.83	1020	1058
Secondary lining	2500	1.76	1.60	1102	1149
Primary support	2300	2.23		1000	

The diffusion coefficient and hydraulic conductivity coefficient in frozen zone are much smaller than those in thawed zone due to the formation of ice lenses, which can be described by the impedance factor I. At this time, the diffusion rate and hydraulic conductivity of unfrozen water inside the surrounding rocks can be determined:

$$I = 10^{10\theta_i} \tag{11}$$

$$D_I(\theta) = \frac{a_2\theta_u^{b_2}}{I} = \frac{a_2\theta_u^{b_2}}{10^{10\theta_i}} \tag{12}$$

$$K_I(\theta) = \frac{a_3\theta_u^{b_3}}{I} = \frac{a_3\theta_u^{b_3}}{10^{10\theta_i}} \tag{13}$$

where $D_I(\theta)$ and $K_I(\theta)$ are the diffusion coefficient and hydraulic conductivity in the frozen zone, respectively, I is the impedance coefficient of ice, $I = 10^{10\theta i}$, θ_i – the volumetric ice content, a_2, b_2, a_3, b_3 are the empirical coefficients, which are $3.56 \cdot 10^{-5}$, 10.86, $3.24 \cdot 10^{-6}$, 3.76, respectively.

Geometric model and boundary conditions

The dimension of the geometric model is shown in fig. 5, the radial depths around the tunnel outline is 50 m. The buried depth is 7.20 m (this value is the buried depth near the tunnel portal). The detailed boundary conditions are as follows.

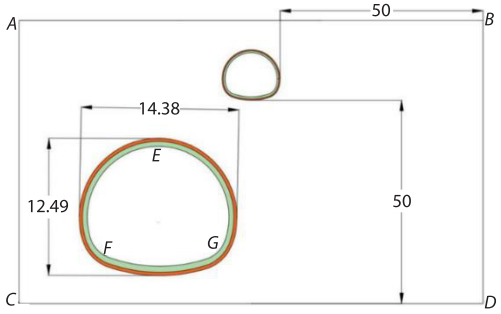

Figure 5. Geometric model [m]

The AB is the process of temperature change outside the tunnel, and can be simplified:

$$T_{ab} = 5.64 + 17.25\sin\left[\frac{2\pi(t-105)}{365}\right] \tag{14}$$

The EFG is the air temperature inside the tunnel, and it varies:

$$T_{efg} = 4.69 + 14.02\sin\left[\frac{2\pi(t-111)}{365}\right] \tag{15}$$

The heat flux of CD at the bottom of the model is taken as 0.06 W/m^2, AC and BD are the adiabatic boundaries. The convective coefficient at the boundary of EFG is 15 W/m^2°C.

Results and discussion

Model verification

In order to verify the accuracy and to improve the convergence of the numerical model, the monitored data and the simulated data are compared in the cold season and in the warm season, respectively. As shown in fig. 6, the ground temperature is approximately constant when the depth is more than 700 cm. In the cold season (July 28, 2019), the ground temperature decreases with depth while its opposite to that in warm season (December 27, 2018). Besides, the monitored data and simulated data of ground temperature at the depth of 50 cm were 22.72 °C and 21.06 °C, respectively on July 28, 2018. While for the monitored data and simulated data of ground temperature at a depth of 1000 cm were –6.02 °C and –7.01 °C, respectively on December 27, 2019. Therefore, it indicates that the simulated data agrees well with the monitored data and the accuracy of the numerical model is credible.

In addition, the temperature of S2 (the central point of the secondary lining), and S3 (the interface between the secondary lining and the primary support) are selected to analyze the temperature change process for monitored data and simulated data. In general, the frozen depth

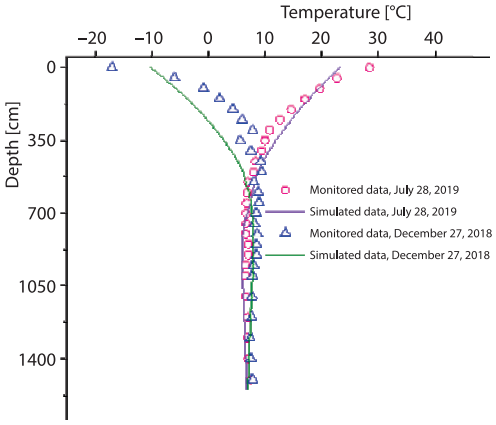

Figure 6. Comparison of ground temperature between monitored data and simulated data

near tunnel portal is relatively greater than that of the middle section of the tunnel. Thus, the cross-section near tunnel portal is the most unfavorable. The monitored data and simulated data at the most unfavorable cross-section are compared to further demonstrate the numerical model is accurate. As shown in fig. 7, the monitored value and simulated value of S2 were –7.02 °C and –6.83 °C, respectively on 16 January, 2019. While these values of S3 were –3.86 °C and –5.18 °C, respectively. Obviously, the numerical model is with high accuracy.

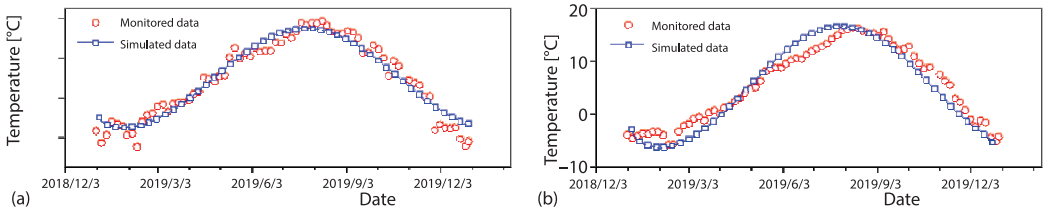

Figure 7. Temperature comparison between monitored data and simulated data at different locations; (a) the center of the second lining and (b) the interface between the secondary lining and the primary support

Evolution process of hydrothermal characteristics

As the formation of free face after the tunnel is excavated, the heat transfer is also enhanced. Based on the numerical model, the temperature behind the primary support at tunnel entrance (near the direction of Hunchun city) is simulated. When the tunnel works at the coldest time in the 30th year, the temperature at five different positions, A, B, C, D, and E are shown in fig. 8, respectively. The temperatures of the positions are –2.96 °C, –3.28 °C, –3.39 °C, –2.19 °C, and –3.10 °C, respectively. Therefore, the point C can be recognized as the most unfavorable position. The dynamic changing process at point C is shown in fig. 9. Clearly, the temperature at this point decreases significantly when the tunnel works in the early three years. The lowest temperature in the cold season is below –0.05 °C during the 30th year, which indicates that frost damage can occur in the studied tunnel without any protected measures.

To visualize the hydrothermal conditions inside the tunnel in the cold season, the temperature, unfrozen water content and ice content are shown in fig. 10. It is evident that temperature rises as depth increases in the radial direction. The temperature of secondary lining surface is –7.0 °C. Besides, the –0.05 °C isotherm locates in the surrounding rocks, which indicates that the surrounding rocks is frozen. The unfrozen water content increases with the increasing of depth along the radial direction and the ice content is opposite to that of unfrozen water content. However, the unfrozen water content and ice content at the surrounding rocks are 12% and 6%, respectively in the 30th year and their total are greater than initial water content (15%), which is caused by water migration from unfrozen zone to frozen zone during freezing process. Water migration results in the accumulation of large amounts of water at the freezing

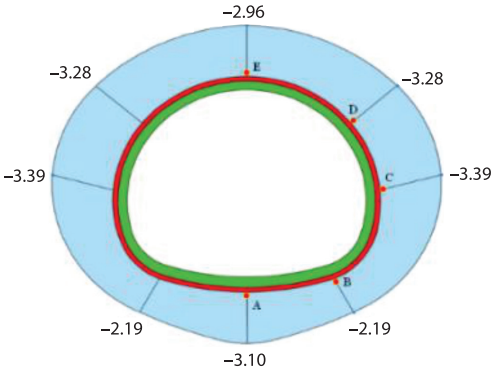

Figure 8. Temperature distribution of surrounding rocks surface when the tunnel works at the coldest time in the 30th year [°C]

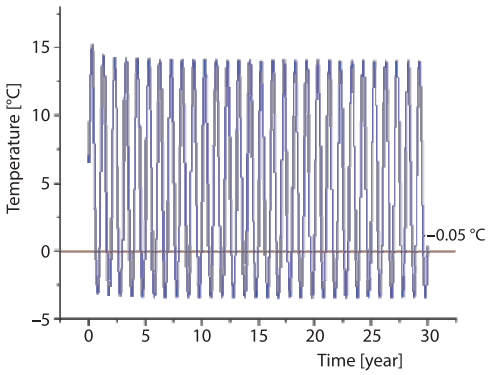

Figure 9. Temperature change at the most unfavorable location

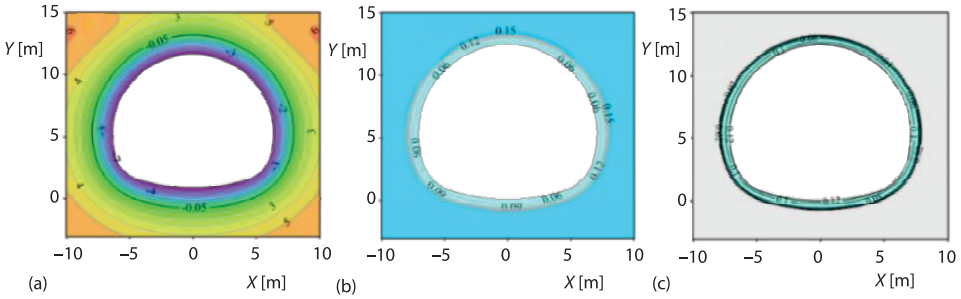

Figure 10. Hydrothermal conditions inside the tunnel when it works in the 30th year; (a) temperature [°C], (b) unfrozen water, and (c) ice content

front. The accumulated water phases into ice at negative temperatures, which further generates frost heave force and accelerates the damages of tunnel structural layers and surrounding rocks. Conversely, the damages can further increase the amount of water migration and lead to more serious damages to occur.

To illustrate the spatio-temporal evolution rules of thermal condition inside the tunnel, fig. 11 depicts the temperature distribution when the tunnel works in the coldest months (February) of the 5th, 15th, and 25th years after construction. The maximum frozen depth reaches 1.59 m in the 5th year and is essentially stays at 1.64 m after the 15th year. The phenomenon has to do with

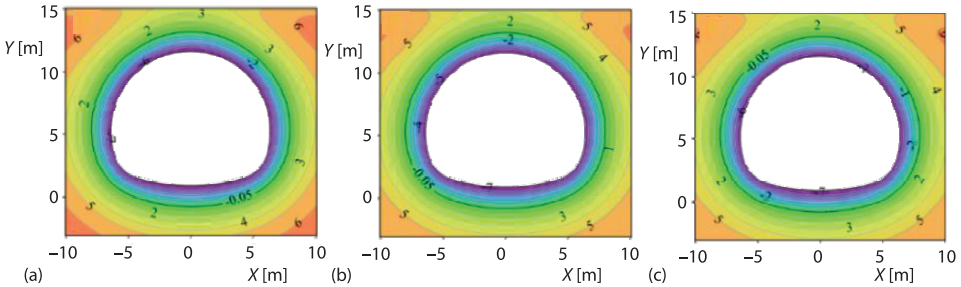

Figure 11. Hydrothermal conditions inside the tunnel when it works in different years; (a) the 5th year, (b) the 15th year, and (c) the 25th year

heat transfer path. The original heat condition around the tunnel is disturbed due to excavation. The heat transfer between tunnel structural layers and atmosphere promotes the development of frozen depth. The temperature inside the surrounding rocks gradually decreased during the cold season, which can be reflected by the distribution of 6 °C isotherm in different years. From figs. 11(a)-11(c), the zone enclosed by the 6 °C isotherm becomes smaller with time, where it completely disappeared in the 15th year and the 25th year at tunnel invert. Meanwhile, the temperature in tunnel structural layers and surrounding rocks is stable after the 15th year, it suggests that the heat balance inside the tunnel is achieved in the year. Therefore, special attention should be focus on the temperatures of tunnel structural layers in the early 15 years after construction.

Anti-freezing design of the tunnel

Based on the section *Evolution process of hydrothermal characteristics*, it is clear that the measures must be employed to protect tunnel from frost damages. As laying the insulation board in tunnel structural layers is a common and effective method based on [27-29]. However, the thickness of insulation board is not same for the different tunnels because the climatic and geological conditions are often various in tunnel site. Therefore, this section aims to determine a reasonable thickness of insulation board (extruded polystyrene panel, XPS) based on numerical analysis. The thickness of XPS board is designed as 3.5 cm and 5 cm, respectively in hydrothermal model to further determine the reasonable thickness of insulation board. It should be noted that the density and heat capacity of the XPS board are 35 kg/m^3 and 800 J/kg°C, respectively.

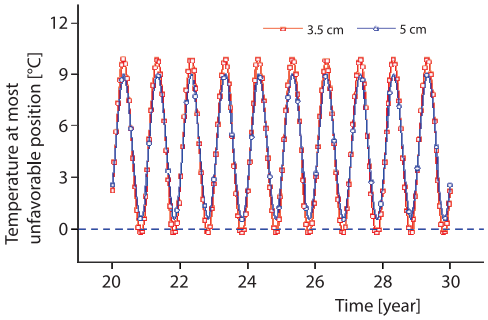

Figure 12. Temperature changing process of surrounding rocks at the most unfavorable position after laying XPS board

Figure 12 shows the temperature change process at the most unfavorable position with different thicknesses of XPS board. As the lowest temperature of surrounding rocks is –0.23 °C in the cold season after laying the XPS board with the thickness of 3.5 cm, the frost damages can still exist. However, when the XPS board with the thickness of 5 cm, the temperature of surrounding rocks is 0.55 °C and is higher than initial freezing temperature (–0.05 °C). Therefore, it suggests that the frost damages disappeared after XPS board is laid inside the tunnel with the thickness of 5 cm.

In addition, the hydrothermal conditions inside the tunnel under different thicknesses of XPS board are shown in figs. 13 and 14, respectively. When the XPS board with the thickness of 3.5 cm, the maximum frozen depth of the tunnel is 0.87 m and the ice distributes on surrounding rocks surface with the maximum value of 4%. When the XPS board with thickness of 5 cm, the maximum frozen depth is 0.60 m and the temperature of the surrounding rocks is positive in the cold season.

Influence of annual mean air temperature

The AMAT is a key parameter for the cold regional engineering because it determines whether the engineering is in endothermic or exothermic state, which is further related to whether frost damage occurs. Some scholars even use the AMAT as an criteria for classification of frozen soil [42]. Besides, the frozen depths are also closely associated with the AMAT, which indicates the influence of AMAT on hydrothermal conditions cannot be neglected for the cold regional tunnels.

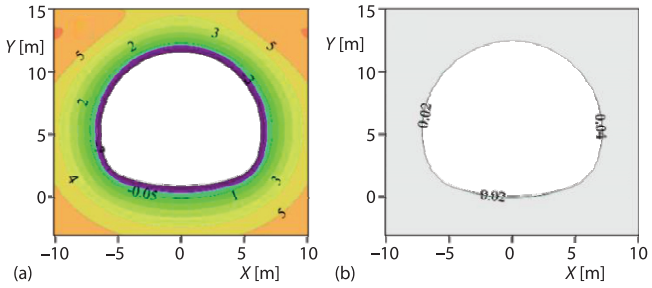

Figure 13. Hydrothermal conditions inside the tunnel after laying XPS board with the thickness of 3.5 cm; (a) temperature [°C] and (b) ice content

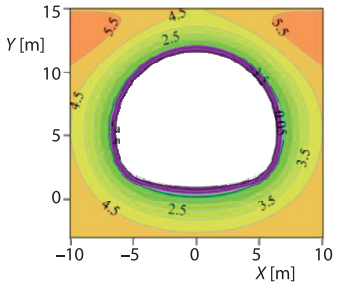

Figure 14. Temperature distribution inside the tunnel after laying XPS board with the thickness of 5 cm [°C]

The AMAT at four meteorological stations from 2014-2019 at Yongji country, Jiaohe city, Dunhua city and Yanji city are listed in tab. 2 (these stations are along the JTHPDL and are adjacent to the studied tunnel). The AMAT of the stations ranged from 6.01-6.79 °C (Yongji country), 4.62-5.72 °C (Jiaohe city), 4.62-5.72 °C (Dunhua city), and 6.02-7.03 °C (Yanji city) from 2014-2019, respectively. Therefore, the AMAT outside the tunnel is determined to be 4-8 °C, respectively (for the boundary condition of AB). At the tunnel site, the air temperature in the monitored cross-section and outside the tunnel from December 2018 and December 2019 are shown in fig. 15, which is 5.7 °C and 4.7 °C, respectively. Obviously, the difference between them is 1 °C. So, the AMAT inside the tunnel is to be determined as 3-7 °C, respectively (for the boundary condition of EFG).

Table 2. The AMAT at different meteorological stations along the JTHPDL

Meteorological station	Yogji country	Jiaohe city	Dunhua city	Yanji city
AMAT [°C]	6.01-6.79	4.62-5.75	4.62-5.72	6.02-7.03

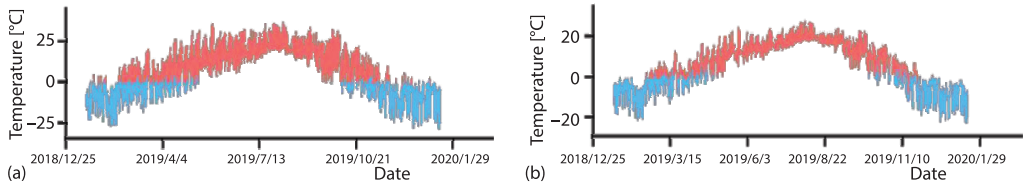

Figure 15. Air temperature changing process; (a) outside the tunnel and (b) in the monitored cross-section

Figure 16 shows the hydrothermal conditions inside the tunnel in cold season when tunnel works in the 30th year. As can be seen that with the increasing of the AMAT, the temperature of tunnel structural layers and surrounding rocks increased simultaneously. When the AMAT is –3 °C, the maximum temperature of surrounding rocks is 3.5 °C. Subsequently, when the AMAT increases from 4-8 °C, the corresponding values are 4.5 °C, 5.5 °C, 6.5 °C, and 7.5 °C, respectively. It is no doubt that the temperature increment of surrounding rocks is at the same growth rate as the AMAT. However, the ice content decreases with the increasing of the AMAT and maximum ice content of surrounding rocks is 11%, which demonstrates the surrounding rocks are frozen. The maximum frozen depth can be derived from the boundary

of –0.05 °C isotherm. When the AMAT increases from 4-8 °C, the maximum frozen depths are 1.93 m, 1.69 m, 1.54 m, 1.31 m, and 1.12 m, respectively. Therefore, the increase of AMAT can alleviate the frost damage inside the tunnel.

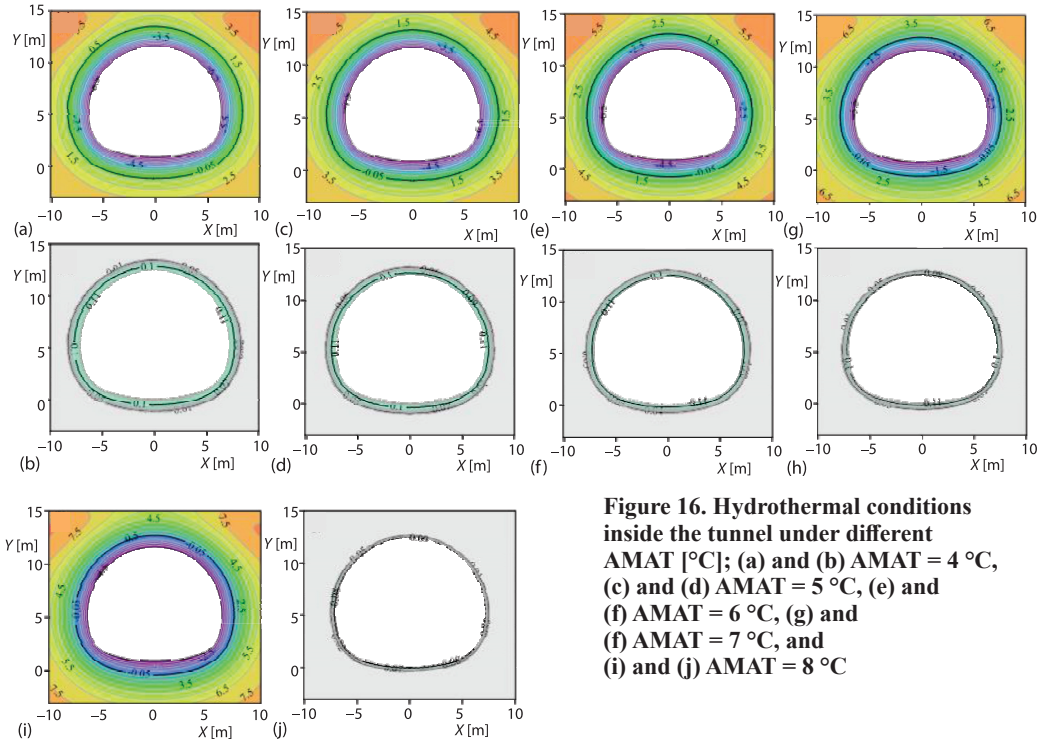

Figure 16. Hydrothermal conditions inside the tunnel under different AMAT [°C]; (a) and (b) AMAT = 4 °C, (c) and (d) AMAT = 5 °C, (e) and (f) AMAT = 6 °C, (g) and (f) AMAT = 7 °C, and (i) and (j) AMAT = 8 °C

Influence of annual range of air temperature

In order to quantitatively analyze the influence of ARAT on hydrothermal conditions of tunnel, the ARAT at four meteorological stations from 2014-2019 are shown in tab. 3. It can be seen that the ARAT ranged from 17.52-21.11 °C (Yongji country), 17.56-21.46 °C (Jiaohe city), 17.56-21.46 °C (Dunhua city), and 15.20-18.40 °C (Yanji city), respectively. Therefore, the ARAT outside the tunnel is determined to be 17-22 °C (for the boundary condition of AB), respectively. The ARAT between monitored section and outside the tunnel is approximately 3 °C according to the monitored data, thus the ARAT inside the tunnel is determined to be 14-19 °C (for the boundary condition of EFG), respectively.

Table 3. The ARAT at different meteorological stations along the JTHPDL

Meteorological station	Yongji country	Jiaohe city	Dunhua city	Yanji city
ARAT [°C]	17.52-21.11	17.56-21.46	17.56-21.46	15.20-18.40

The hydrothermal conditions inside the tunnel under different ARAT are shown in fig. 17. Taking the ARAT is 17 °C as an example to illustrate the hydrothermal conditions of tunnel structural layers and surrounding rocks. The temperature on secondary lining surface is –7.5 °C, and the temperatures of secondary lining and primary support are below –0.05 °C at this time. The maximum ice content of surrounding rocks is 11%. Then with the increase of ARAT,

the temperature significantly decreases and the zones containing with ice also expands. It indicates that maximum frozen depth is continuously increasing. When the ARAT increases from 17-22 °C, the maximum frozen depths are 1.60 m, 1.77 m, 1.84 m, 1.94 m, and 2.01 m, respectively. Obviously, the frozen zone expands with the increase of ARAT.

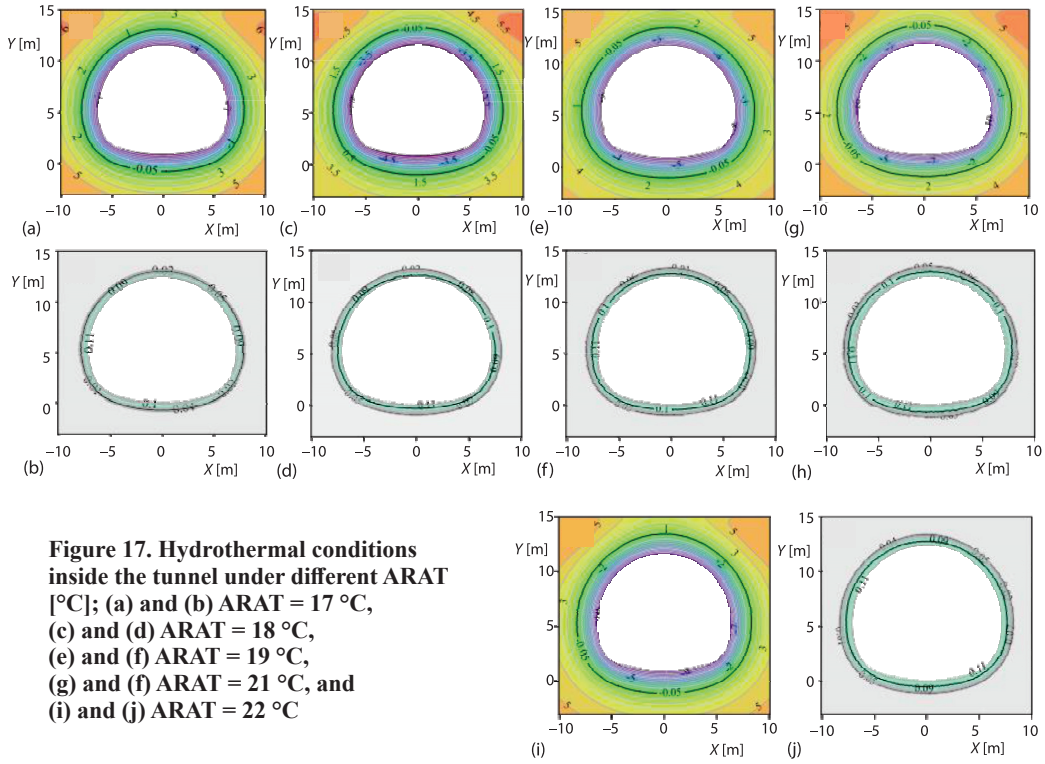

Figure 17. Hydrothermal conditions inside the tunnel under different ARAT [°C]; (a) and (b) ARAT = 17 °C, (c) and (d) ARAT = 18 °C, (e) and (f) ARAT = 19 °C, (g) and (f) ARAT = 21 °C, and (i) and (j) ARAT = 22 °C

Conclusions

Based on in-situ monitored data and numerical simulation, the hydrothermal conditions considering climatic change of a high speed railway tunnel are analyzed. The most unfavorable position of the tunnel is recognized and the reasonable thickness of insulation board to prevent frost damage is determined. The conclusions are as follows.

- Under unprotected conditions, with the increase of service time of the tunnel, the temperature of structural layer gradually decreased. When the tunnel works in the 30th year, the unfrozen water content and ice content of surrounding rocks can reach 12% and 6%, respectively. The most unfavorable position occurs at the tunnel sidewall and with the maximum frozen depth of 1.64 m. Some measures must be taken to avoid frost damage for the tunnel.
- When the XPS board is laid in tunnel structural layers with the thickness of 3.5 cm and 5 cm, respectively, the temperature of surrounding rocks at the most unfavorable position is –0.23 °C and 0.55 °C, respectively in the cold season. Therefore, to avoid the frost damages that occur inside the tunnel, the XPS board with the thickness of 5 cm should be adopted.
- The AMAT and the ARAT have a significant influence on the hydrothermal conditions inside the tunnel. When the AMAT increases from 4-8 °C, the temperature of the tunnel structural layers developed as quickly as surrounding rocks, and the maximum frozen depths are 1.93 m, 1.69 m, 1.54 m, 1.31 m, and 1.12 m, respectively. With the increases of the ARAT,

the temperature of the tunnel structural layers and surrounding rocks decreases significantly and the zones containing with ice expands accordingly. When the ARAT increases from 17-22 °C, the maximum frozen depths are 1.60 m, 1.77 m, 1.84 m, 1.94 m, and 2.01 m, respectively.

Acknowledgment

This study was financially supported by the Heilongjiang Provincial Postdoctoral Science Foundation (Grant No. LBH-Z22073) and the Open Foundation of the Research Center for Human Geography of Tibetan Plateau and Its Eastern Slope (Grant No. RWDL2022-YB003). The authors would like to thank the anon-ymous reviewers of this paper for their constructive comments.

Contribution

Authors Haiqiang Jiang and Tengfei Zhou contributed equally to this work.

References

[1] Bates, R. E., Bilello, M. A., Defining the Cold Regions of the Northern Hemisphere, Technical Report No. 178, U. S. Army Cold Regions Research and Engineering Laboratory, Hanover, N. H., USA, 1966
[2] Xing, R. J., *et al*., Long-Term Temperature Monitoring of Tunnel in High-Cold and High-Altitude Area Using Distributed Temperature Monitoring System, *Measurement*, *95* (2017), Jan., pp. 456-464
[3] Chen, R. S., *et al*., Cold Regions in China (in Chinese), *Cold Reg. Sci. Tech.*, *45* (2006), 2, pp. 95-102
[4] Jiang, H. Q., *et al*., Numerical Modelling of Thermal Stability for a Water Retaining Wall in Permafrost Regions, *Thermal Science Engineering Progress*, *36* (2022), 101494
[5] Liu, H., *et al*., Study of Design of Filling Material and Setting Anti-Frost Layer for High-Speed Railway Roadbed in Seasonally Frozen Region, *Chinese Journal of Rock Mechanics and Engineering*, *30* (2011), 12, pp. 2549-2557
[6] Niu, F. J., *et al*., Permafrost Characteristics of the Qinghai-Tibet Plateau and Methods of Roadbed Construction of Railway, *Acta Geological Sinica*, *82* (2008), 5, pp. 949-958
[7] Ma, W., *et al*., Basic Research on the Major Permafrost Projects in the Qinghai-Tibet Plateau, *Advance in Earth Sciences*, *27* (2012), 11, pp. 1185-1191
[8] Luo, J., *et al*., Field Experimental Study on Long-Term Cooling and Deformation Characteristics of Crushed-Rock Revetment Embankment at the Qinghai-Tibet Railway, *Applied Thermal Engineering*, *139* (2018), July, pp. 256-263
[9] Zhang, S. Z., *et al*., Risk Assessment of Engineering Diseases of Embankment-Bridge Transition Section for Railway In Permafrost Regions, *Permafrost Periglacial Process*, *33* (2022), 1, pp. 46-62
[10] Miao, Q., *et al*., Comparing Frost Heave Characteristics in Cut and Embankment Sections along a High-Speed Railway in Seasonally Frozen Ground of Northeast China, *Cold Regions Science and Technology*, *170* (2020), 102921
[11] Cao, S. D., *et al*., Experimental Study on the Temperature Field of Cold Region Tunnel under Various Groundwater Seepage Velocities, *Advances in Civil Engineering*, *2020* (2020), ID6695099
[12] Zhou, X. H., *et al*., Discussion of Anti-Freeze and Frost Resistance of Shallow Buried Tunnels in High Latitude Cold Region (in Chinese), *Journal of Glaciology and Geocryology*, *38* (2016), 1, pp. 121-128
[13] Zhou, Y. F., *et al*., Optimal Design of Central Drainage Ditch Buried Depth for Highway Tunnel in Seasonally Frozen Region, *KSCE Journal of Civil Engineering*, *2*6 (2022), 4, pp. 1674-1682
[14] Wang, D. Y., *et al*., Safety Evaluation and Action Mechanism of Frost Heave with Local Water Storage in Shallow Tunnel (in Chinese), *Journal of Traffic and Transportation Engineering*, *20* (2020), 3, pp. 40-50
[15] Zhao, P. Y., *et al*., Field Measurement of Air Temperature in a Cold Region Tunnel in Northeast China, *Cold Regions Science and Technology*, *171* (2020), 102957
[16] Jun, K. J., *et al*., Field Measurement of Temperature Inside Tunnel in Winter in Gangwon, Korea, *Cold Regions Science and Technology*, *143* (2017), Nov., pp. 32-42
[17] Tian, S. M., *et al*., Development and Prospect of Railway Tunnels in China(Including Statistics of Railway Tunnels in China by the End of 2020) (in Chinese), *Tunnel Construction*, *41* (2021), 2, pp. 308-325
[18] Jiang, H. Q., *et al*., Thermal Characteristics Investigation of a High-Speed Railway Tunnel by Field Monitoring in Northeast of China, *Transportation Geotechnic*., *30* (2021), 100615

[19] Chang, H. T., *et al*., Monitoring and Analysis of the Temperature Field of a Cold-Region Highway Tunnel Considering the Traffic-Induced Thermal Effect, *Case Studies in Thermal Engineering*, *40* (2022), 102482
[20] Liu, W. W., *et al*., Analytical Solution for 3-D Radial Heat Transfer in a Cold-Region Tunnel, *Cold Regions Science and Technology*, *164* (2019), 102787
[21] Zhao, P. Y., *et al.*, Long-Term, Real-Time And Multi-Channel Distributed Temperature Monitoring System for Tunnels *in Cold Regions, Measurement Science and Technology, 30* (2019), 6, 065105
[22] Yan, Q. X*., et al*., Numerical Investigation of Heat-Insulating Layers in a Cold Region Tunnel, Taking into Account Air-Flow and Heat Transfer, *Applied Sciences-Basel*, *7* (2017), 7, 679
[23] Jiang, H. Q., *et al*., Numerical Studies for the Thermal Regime of a High-Speed Railway Tunnel Considering Piston Action on Seasonally Frozen Regions, *Journal of Thermal Science and Engineering Applications*, *14* (2022), 9, 091012
[24] Jiang, H. Q., *et al*., Numerical Analysis of Heat Transfer Between Air Inside and Outside the Tunnel Caused by Piston Action, *International Journal of Thermal Sciences*, *170* (2021), 107164
[25] Yang, T. J., *et al*., Numerical Analysis on Thermo-Hydro-Mechanical Coupling of Surrounding Rocks in Cold Region Tunnels, *Journal of Northeastern University*, *40* (2019), 8, pp. 1178-1184
[26] Jiang, H. Q., *et al*., Experimental Investigation on Performance Degradation of Insulation Materials Induced By Freeze-Thaw Cycles and Its Applications, *Construction and Building Materials*, *350* (2022), 128844
[27] Yuan, K. K., High-Strength and Heat Insulation Foam Concrete: Developing and Applying in Cold Region Tunnel (in Chinese), *Journal of Glaciology and Geocryology*, *38* (2016), 2, pp. 438-444
[28] Lai, J. X., *et al*., Freeze-Proof Method and Test Verification of a Cold Region Tunnel Employing Electric Heat Tracing, *Tunnelling and Underground Space Technology*, *60* (2016), Nov., pp. 56-65
[29] Wang, R. Y., *et al.*, Model Test of Temperature Field of Tunnel in Cold Region and Air Curtain Insulation Measures, *China Railway Science*, *42* (2021), 3, pp. 70-82
[30] ***, TB 10601-2009, Code for Engineering Survey of High Speed Railway (in Chinese)
[31] Luo, J., *et al.*, Variations in the Northern Permafrost Boundary over the Last Four Decades in the Xidatan Region, Qinghai-Tibet Plateau, *Jounral of Materials Science*, *15* (2018), 4, pp. 765-778
[32] Ran, Y. H., *et al*., Climate Warming over the Past Half Century Has Led to Thermal Degradation of Permafrost on the Qinghai-Tibet Plateau, *Cryosphere*, *12* (2018), 2, pp. 595-608
[33] Jin, H. J., *et al*., Degradation of Permafrost in the Da and Xiao Hinggan Mountains, Northeast China, and Preliminary Assessment of Its Trend (in Chinese), *Journal of Glaciology and Geocryology*, *28* (2006), 4, pp. 467-476
[34] He, R. X., *et al.*, Changes in the Permafrost Environment under Dual Impacts of Climate Change and Human Activities in the Hola Basin, Northern Da Xing'anling Mountains, Northeast China, *Land Degradation and Development*, *33* (2022), 8, pp. 1219-1234
[35] Kuznetsov, G. V., *et al*., Heat Transfer in a Two-Phase Closed Thermosyphon Working in Polar Regions, *Thermal Science Engineering Progress*, *22* (2021), 100846
[36] Luo, J., *et al*., Abrupt Increase in Thermokarst Lakes on the Central Tibetan Plateau over the Last 50 Years, *Catena*, *217* (2022), 106497
[37] Jin, X. Y., *et al.,* Impacts of Permafrost Degradation on Hydrology and Vegetation in the Source Area of the Yellow River on Northeastern Qinghai-Tibet Plateau, Southwest China, *Frontiers of Earth Science*, *10* (2022), 845824
[38] ***, Basic information of Gaotai tunnel, https://www.wikipedia.org
[39] ***, JJG229-2010, National Metrological Verification Regulation of People's Republic of China-Industry Platinum and Copper Resistance Thermometers (in Chinese)
[40] Jiang, H. Q., Investigation on Evolution Characteristics of Temperature Field and Anti-Freezing Measures of High-Speed Railway Tunnel in Cold Regions (in Chinese), Ph. D. thesis, South China University of Technology, Guangzhou, China, 2021
[41] Zhang, X. F., *et al.*, Forecast Analysis of the Refreezing of Kunlun Mountain Permafrost Tunnel on Qing-Tibet Railway in China, *Cold Regions Science and Technology*, *39* (2004), 1, pp. 19-31
[42] Xv, X. Z., *et al*., Frozen Soil Physics, Science Press., Beijing, China, 2001

Paper submitted: January 22, 2023
Paper revised: February 8, 2023
Paper accepted: March 24, 2023